Nanochem Res 2(2): 188-197, Summer and Autumn 2017

RESEARCH PAPER

Bi-functional $NaLuF_4$:Gd^{3+}/Yb^{3+}/Er^{3+} nanocrystals: Hydrothermal synthesis, optical and magnetic properties

Jigmet Ladol, Heena Khajuria, Manesh Kumar, Haq Nawaz Sheikh *

Department of Chemistry, University of Jammu, Jammu Tawi, India

ARTICLE INFO

Article History:
Received 16 April 2017
Accepted 20 June 2017
Published 1 July 2017

Keywords:
Fluorides Nanocrystals
Luminescence
Magnetic Properties
X-Ray Diffraction

ABSTRACT

Magnetic-fluorescent lanthanide doped sodium lutetium fluoride ($NaLuF_4$:Yb^{3+}/Er^{3+}/Gd^{3+}) nanocrystals were synthesized via facile hydrothermal method by varying concentration of Gd^{3+}. Powder X-ray powder diffraction (PXRD), scanning electron microscopy (SEM), transmission electron microscopy (TEM), energy dispersive X-ray spectroscopy (EDS), particle size by dynamic light scattering (DLS), photoluminescence (PL) and magnetic studies were used to characterize the structural, optical and magnetic properties of these nanocrystals. Powder X-ray diffraction results signified good crystallinity and effective doping in sodium lutetium fluoride nanocrystals. The SEM and TEM micrographs defined their flower like morphology. The EDS was performed to investigate the presence of dopant. The emission intensities of the prepared samples are strongly controlled by particle sizes which are influenced by co-doping $NaLuF_4$ nanocrystals with varying concentration of Gd^{3+}. Besides the efficient optical properties, Gd^{3+} doped $NaLuF_4$ nanocrystals exhibited paramagnetic behavior at room temperature with magnetization of up to 8.24×10^{-3} emu g^{-1} at 15 kOe.

How to cite this article
Ladol J, Khajuria H, Kumar M, Nawaz Sheikh H. Bi-functional $NaLuF_4$:Gd^{3+}/Yb^{3+}/Er^{3+} nanocrystals: hydrothermal synthesis, optical and magnetic properties. Nanochem Res, 2017; 2(2):188-197. DOI: 10.22036/ncr.2017.02.005

INTRODUCTION

Lanthanide ion-doped rare-earth fluorides have gained considerable attention because of their potential applications in the fields such as photodynamic therapy, three-dimensional displays, catalysis, solid-state lasers, low-intensity IR imaging and other optical devices arising from intra f-f transitions [1-5]. Among the various host matrices for Ln^{3+} ions, fluoride host lattices have high chemical and thermal stability and also possess low phonon energies to reduce non-radiative relaxations, thereby improving the luminescence of the optically active dopants [6-8]. Low-energy phonons and high ionicity are highly desirable properties for efficient luminescence. Multifunctional nanocrystals possessing both magnetic and fluorescent properties have received increasing attraction in the past decade [9-12]. The synthesis of magnetic nanoparticles (MNPs) have attracted much attention due to their excellent physico-chemical properties. During the last few years, efficient routes have been devised for the synthesis of shape-controlled and highly stable functionalized polyethylenimine (PEI), β-cyclodextrin and Succinate grafted PEI nanocomposites with magnetic ferrites [13-17]. These functionally modified MNPs found their applications in dye degradations [18, 19], drug delivery [20-22] and as magnetically separable efficient organic catalyst, used for green oxidation of alcohols [23-27], oxidation of hydrocarbons in the presence of H_2O_2 [28], anti-oxidant [29] and synthesis of polyhydroquinoline derivatives [30, 31]. Paramagnetic Gd^{3+} doped host metal fluoride, when combined with luminescent lanthanide metal ion gives a wide range of applications including

* Corresponding Author Email: *hnsheikh@rediffmail.com*

magnetic resonance imaging, drug target, various medical diagnostics, cancer therapy, recording material, catalysis and magneto-optics devices [32-38]. $NaLuF_4$ is considered as one of the promising host fluoride nanomaterials based on the physical, chemical and optical properties of the Lu^{3+} ion [39-41]. Although the Lu-based host nanomaterials exhibit promising photoluminescence behaviour [42], limited reports are there on the study of the bi-functional optical and magnetic $NaLuF_4$ nanomaterials. In addition, the optical, magnetic, physical, and chemical properties of nanocrystals depend highly on their structure, size, and shape [43-45]. Therefore, it is very important to synthesize nanocrystals with well controlled size and structure. Lanthanide doped luminescent materials have been synthesized using various methods such as thermal decomposition [46], co-precipitation [47], hydro(solvo)thermal [48,49], ionic liquid-based synthesis [50], microemulsion assisted [51] and microwave-assisted synthesis [52]. Among these methods, hydrothermal synthesis allows excellent control over particle size, shape, distribution and crystallinity of material. The synthesis is conducted in a stainless autoclave using water as a solvent and nanocrystal formation process occurs under high autogenous pressure at a synthesis temperature above the boiling point of the solvent or mixed solution.

In this paper, we report the development of a hydrothermal method for the preparation of multifunctional magnetic-fluorescent lanthanide doped sodium lutetium fluoride ($NaLuF_4:Gd^{3+}/Yb^{3+}/Er^{3+}$) nanocrystals. Luminescence efficiency and paramagnetic behaviour of doped $NaLuF_4$ nanocrystals have been studied which are promising for use as luminescent probes in biological labeling and imaging technology.

EXPERIMENTAL

Materials and instrumentation

Lutetium(III) nitrate hydrate $Lu(NO_3)_3.H_2O$ (99.9%), gadolinium(III) nitrate hexahydrate $Gd(NO_3)_3.6H_2O$ (99.9%), ytterbium(III) nitrate hexahydrate $Yb(NO_3)_3.6H_2O$ (99.9%) and erbium(III) nitrate hexahydrate $Er(NO_3)_3.6H_2O$ (99.9%) were purchased from sigma Aldrich. Sodium hydroxide (NaOH), trisodium citrate ($Na_3C_6H_5O_7$) and ammonium tetrafluoroborate (NH_4BF_4) were purchased from Alfa Aesar and used as received without further purification. Doubly distilled water was used for preparing aqueous solutions.

The phase structure and size of the as-prepared samples were determined from powder X-ray diffraction (PXRD) using D8 X-ray diffractometer (Bruker) at a scanning rate of 12^o min^{-1} in the 2θ range from 10^o to 70^o, with Cu Kα radiation (λ=0.15405 nm). Scanning electron microscopy (SEM) analysis of the samples was recorded on FEI Nova NanoSEM 450. High resolution transmission electron microscopy (HRTEM) was recorded on Tecnai G2 20 S-TWIN Transmission Electron Microscope with a field emission gun operating at 200 kV. Samples for TEM measurements were prepared by evaporating a drop of the colloid onto a carbon-coated copper grid. The energy spectra were obtained by the energy-dispersive X-ray spectrum equipped on a Transmission Electron Microscope. The particle size of each compound was determined by DLS technique using Zetasizer Nano ZS-90 (Malvern Instruments Ltd., Worcestershire, UK). The photoluminescence excitation and emission spectra were recorded at room temperature using Agilent Cary Eclipse Fluorescence Spectrophotometer equipped with a Xenon lamp that was used as an excitation source. The magnetization as a function of an applied field for Gd^{3+} doped in core/shell nanoplates was recorded using vibrating sample magnetometer (VSM), Lakeshore 7410. All the measurements were performed at room temperature.

Preparation

The pure/undoped $NaLuF_4$ and $NaLuF_4$:20%Yb^{3+} /2%Er^{3+}/xGd^{3+} (x = 0%, 10%, 20%, 30%, and 45%) nanocrystals were synthesized by a hydrothermal method using trisodium citrate as a structure directing agent. The typical synthesis involved the addition of 10 mL of ethanol to 2 mL of an aqueous solution containing 1.2 g of NaOH under stirring to form a homogeneous solution. Then, 10 mL of trisodium citrate was added into the above solution under continuous stirring. Subsequently, 2 mmol $RE(NO_3)_3$ (RE = Lu, Yb, Er and Gd with designed molar ratios) and 5 mL of 4 mmol aqueous NH_4BF_4 solutions were added under constant vigorous stirring for 30 minutes. The resulting solution was transferred into a 50 mL stainless Teflon-lined autoclave, which was operated at 170 °C for 24 hours. As autoclave was cooled to room temperature naturally, the precipitates were separated by centrifugation, washed with deionized water and ethanol in sequence, and then collected nanocrystals were dried at 60 ^{o}C for 12 hours.

RESULTS AND DISCUSSION

Crystalline structure and morphology

The crystal structures and the phase purity of the as-prepared nanocrystals were examined by powder X-ray diffraction (PXRD) analysis. The diffraction peaks of the samples depicted in Fig. 1 correspond to the hexagonal and cubic phase (marked with stars) of $NaLuF_4$ (JCPDS card no. 27-0726). It can also be seen that the diffraction peaks of the $NaLuF_4$ samples are very sharp and strong, indicating that products with high crystallinity have been obtained. High crystallinity is important for phosphors, because it generally means less traps and stronger luminescence. It should be noted that the distinctly strengthen intensities of typical peaks indicate the ideal growth orientation of the samples. The lattice parameters calculated using indexing method are in good agreement with those reported in the literature for bulk $NaLuF_4$; a =5.901 Å, c = 3.453 Å (JCPDS card no. 27-0726) are shown in Table 1 [53]. The slight change in the value of lattice constants may be caused by the addition of the dopant metal ion. The diffraction peaks gradually broaden on increasing the Gd^{3+} concentration, indicating a reduction of particle size, which is further confirmed by modified Scherrer's equation. The broadening of the diffraction peaks indicates that the sizes of the undoped and doped $NaLuF_4$ nanocrystals are at the nanoscale.

Table 1 Calculated crystallite size and lattice parameters.

Sample	Lattice parameters (Å)		Crystallite structure (nm)
	a = b	c	Modified Scherrer's method
$NaLuF_4$	5.910	3.464	120
$NaLuF_4$:Yb^{3+}/Er^{3+}	5.922	3.466	115
$NaLuF_4$:Yb^{3+}/Er^{3+}/10%Gd^{3+}	6.051	3.520	107
$NaLuF_4$:Yb^{3+}/Er^{3+}/20%Gd^{3+}	6.141	3.614	93
$NaLuF_4$:Yb^{3+}/Er^{3+}/30%Gd^{3+}	6.351	4.100	85
$NaLuF_4$:Yb^{3+}/Er^{3+}/45%Gd^{3+}	6.446	4.232	82

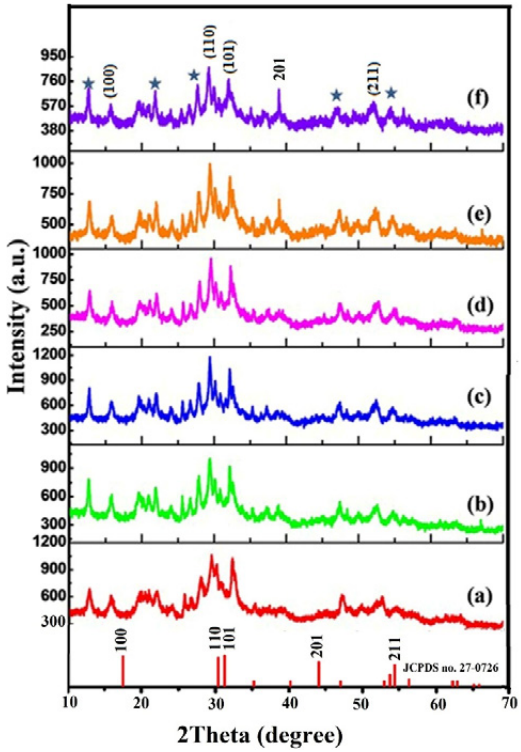

Fig. 1 PXRD patterns for (a) undoped and 20%Yb^{3+}/2%Er^{3+} doped $NaLuF_4$ nanocrystals with different Gd^{3+} contents: (b) 0% (c) 10% (d) 20% (e) 30% (f) 45%

The average crystallite size of these nanocrystals was calculated according to the modified Scherrer's equation

$$\ln\beta(°)=\ln K\lambda(nm)/L(nm)+\ln 1/\cos\theta(°)$$

where, L is the crystallite size, λ is the wavelength of the Cu Kα radiant, λ=0.15405 nm, β is the full-width at half-maximum (fwhm) of the diffraction peak, θ is the diffraction angle and K is the Scherrer constant equals to 0.89. If we plot the results of lnβ against ln1/cosθ, then a straight line with the slope of around one and the intercept of lnK/L was obtained. After getting the intercept, the exponential of the intercept was obtained:

$$e^{\ln K\lambda/L} = K\lambda(nm)/L(nm)$$

Having the value of K and λ, a single value of L in nanometer was calculated. All the major peaks were used to calculate the average crystallite size of the synthesized nanocrystals.

The morphology of the synthesized undoped $NaLuF_4$ and $NaLuF_4$:20%Yb^{3+}/2%Er^{3+}/xGd^{3+} (x = 0%, 10%, 20%, 30%, and 45%) nanocrystals was investigated by using electron microscope studies such as scanning electron microscopy (SEM) and transmission electron microscopy (TEM). Fig. 2 shows SEM images of the synthesized undoped, 20%Yb^{3+}/2%Er^{3+} doped and 20%Yb^{3+}/2%Er^{3+}/x%Gd^{3+} doped $NaLuF_4$ nanocrystals. It is evident from the SEM images that the synthesized particles have flower-shaped morphology and

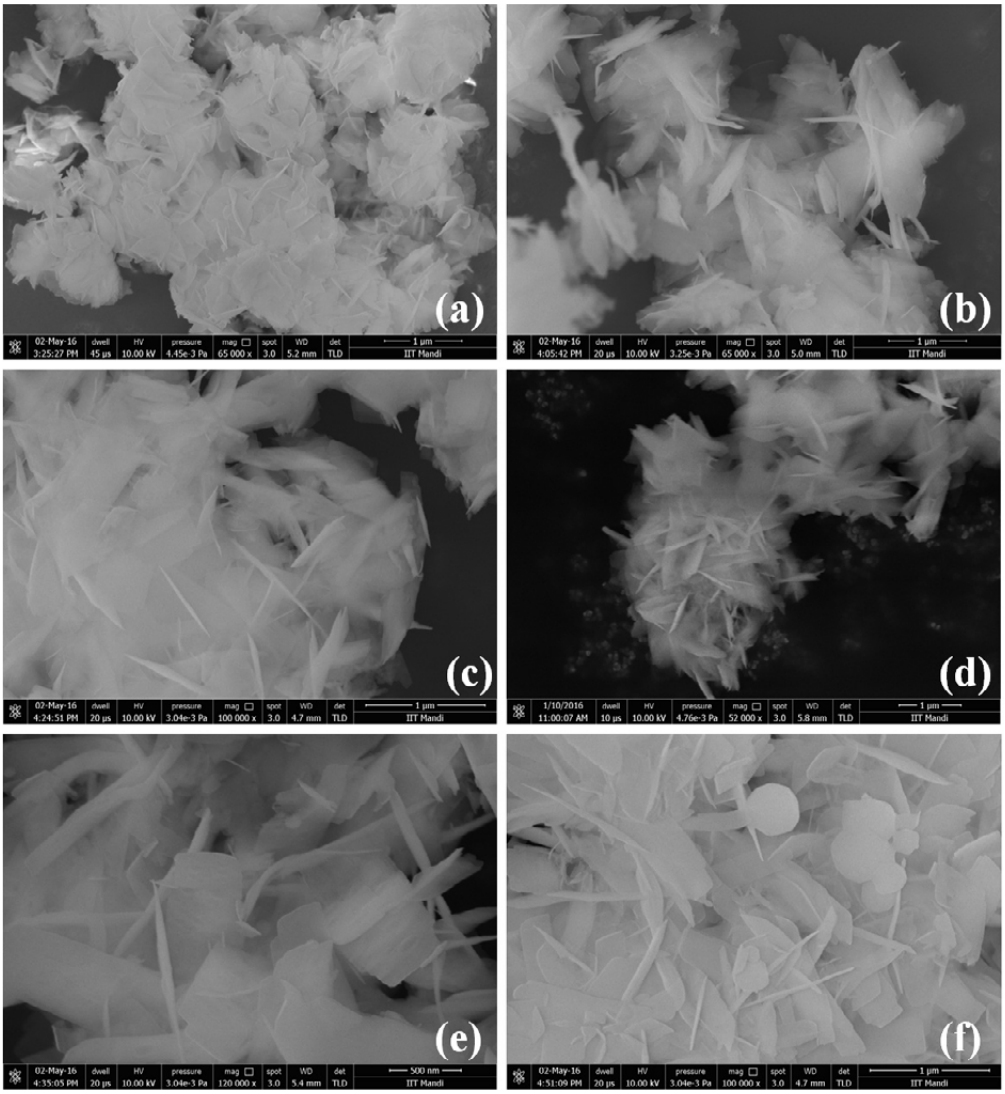

Fig. 2 SEM images for (a) undoped and 20%Yb^{3+}/2%Er^{3+} doped $NaLuF_4$ nanocrystals with different Gd^{3+} contents: (b) 0% (c) 10% (d) 20% (e) 30% (f) 45%

do not show any aggregation of particles. SEM images also indicate that the surface morphology of nanocrystals do not cause any obvious change with the nature of dopant. Fig. 3 shows the high resolution TEM images of the synthesized undoped, 20%Yb^{3+}/2%Er^{3+} doped and 20%Yb^{3+}/2%Er^{3+}/x%Gd^{3+} doped $NaLuF_4$ nanocrystals.

Energy dispersive X-ray analysis spectroscopy was performed to investigate the presence of dopant in the doped $NaLuF_4$ nanocrystals. Fig. 4 show the energy dispersive spectra of the Yb^{3+}/Er^{3+} doped $NaLuF_4$ nanocrystals and Yb^{3+}/Er^{3+}/x%Gd^{3+} doped $NaLuF_4$ nanocrystals. It has been found that the elements ytterbium, erbium, fluorine, sodium and lutetium exist in the Yb^{3+}/Er^{3+} doped $NaLuF_4$ nanocrystals whereas gadolinium presents in the respective synthesized Yb^{3+}/Er^{3+}/Gd^{3+} doped $NaLuF_4$ nanocrystals. These results confirm the doping in $NaLuF_4$ nanocrystals. There is no impurity phase detected in the EDS spectra showing the formation of pure product.

Particle size by DLS technique

The particle size of the synthesized undoped $NaLuF_4$ and $NaLuF_4$:20%Yb^{3+}/2%Er^{3+}/xGd^{3+} (x = 0%, 10%, 20%, 30%, and 45%) nanocrystals was also examined using DLS technique. The nanocrystals were suspended in aqueous medium as colloidal solution after mild sonication for 15 minutes. As observed from Fig. 5, the DLS measurements show

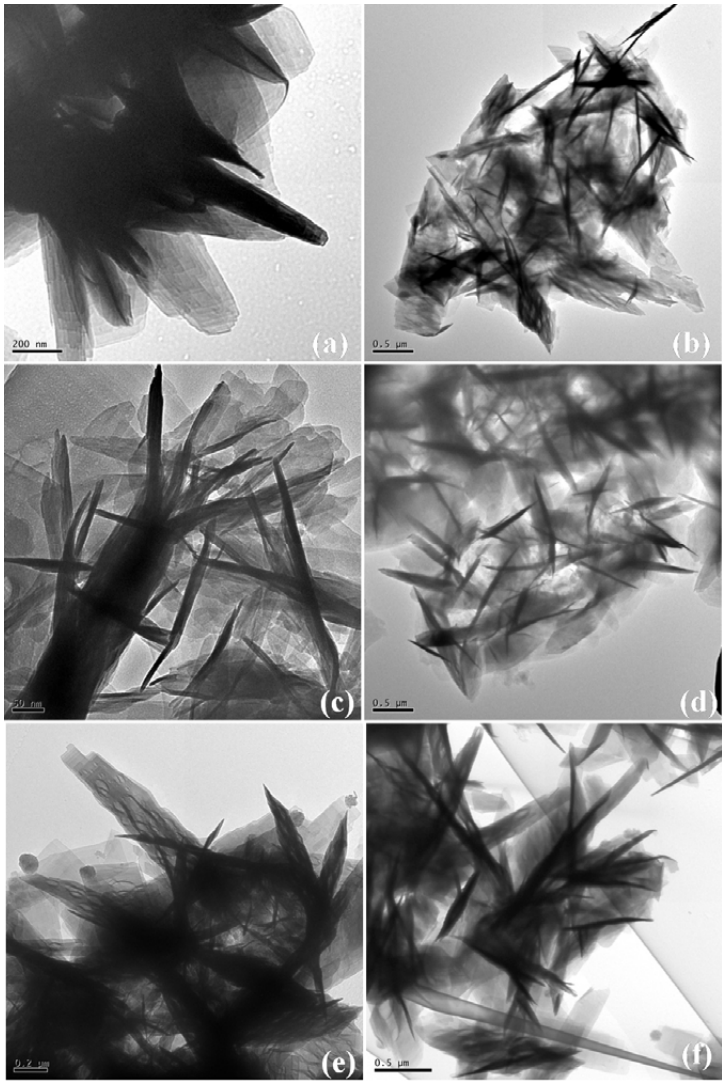

Fig. 3 TEM images for (a) undoped and 20%Yb^{3+}/2%Er^{3+} doped $NaLuF_4$ nanocrystals with different Gd^{3+} contents: (b) 0% (c) 10% (d) 20% (e) 30% (f) 45%

mean particle size of 156, 137, 123, 98, 90 and 85 nm for the synthesized undoped $NaLuF_4$ and $NaLuF_4$:20%Yb^{3+}/2%Er^{3+}/xGd^{3+} (x = 0%, 10%, 20%, 30%, and 45%) nanocrystals, respectively. The size calculated by DLS technique is usually larger than that calculated from PXRD data. The anomaly in sizes is due to surface solvation and agglomeration of the particles.

Absorption spectra

The controlling and tuning of band edge emission and surface traps state emission of $NaLuF_4$:20%Yb^{3+}/2%Er^{3+} and $NaLuF_4$:20%Yb^{3+}/2%Er^{3+}/xGd^{3+} nanocrystals are very important to realize the tunable optical properties and laser emissions. Fig. 6 shows the UV–Vis absorption spectra of the synthesized $NaLuF_4$:20%Yb^{3+}/2%Er^{3+} and $NaLuF_4$:20%Yb^{3+}/2%Er^{3+}/x%Gd^{3+} (x = 20% and 45%) nanocrystals. For recording the absorption spectra, the as-prepared doped $NaLuF_4$ nanocrystals were dispersed in deionized water by ultrasonication for 15 minutes. The prominent absorption edge for as-prepared nanocrystals was observed at around 980 nm and some other less intense absorption edges were also observed lying in the range of 350- 900 nm. The optical band gap of the synthesized nanocrystals was calculated according to the relationship between the optical band gap (E_g) and wavelength (λ) (i.e., E_g = 1240/λ). The band gap thus calculated was found to be 5.1 eV.

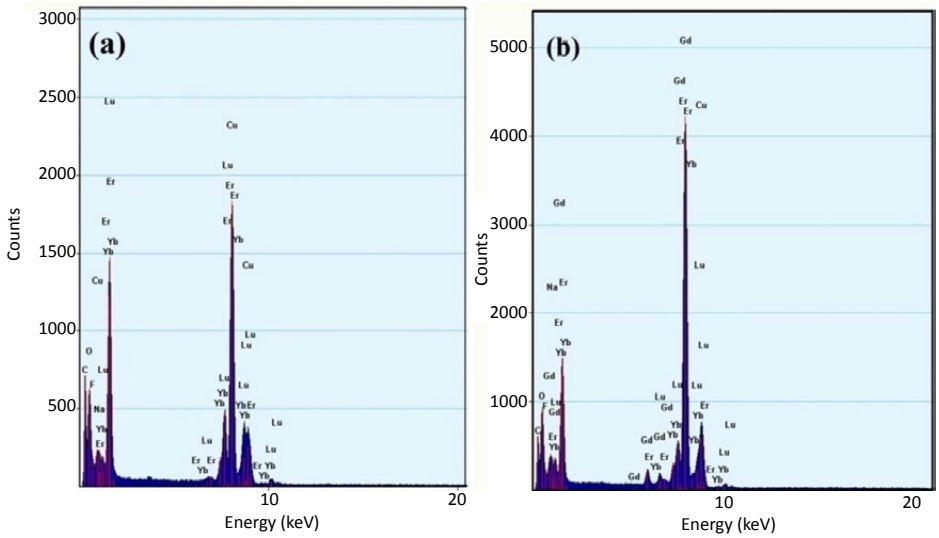

Fig. 4 EDS spectra for (a) 20%Yb^{3+}/2%Er^{3+}:$NaLuF_4$ (b) Yb^{3+}/Er^{3+}/Gd^{3+} doped $NaLuF_4$ nanocrystals

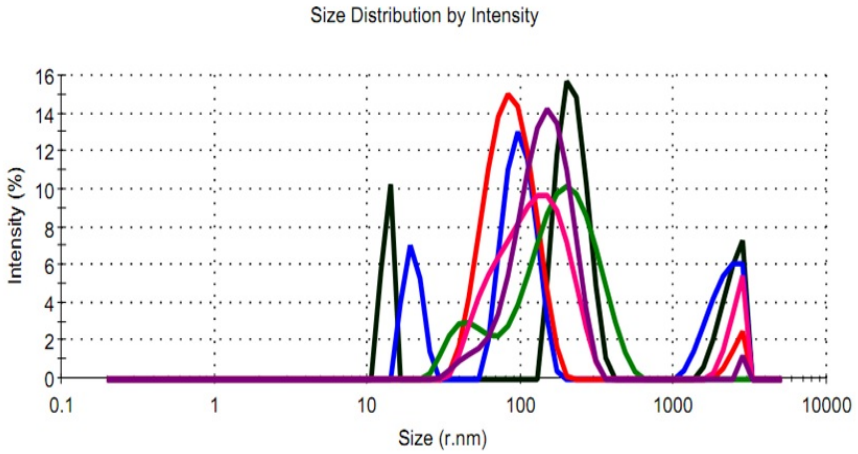

Fig. 5 Particle size by DLS for (a) undoped and 20%Yb^{3+}/2%Er^{3+} doped $NaLuF_4$ nanocrystals with different Gd^{3+} contents: (b) 0% (c) 10% (d) 20% (e) 30% (f) 45%

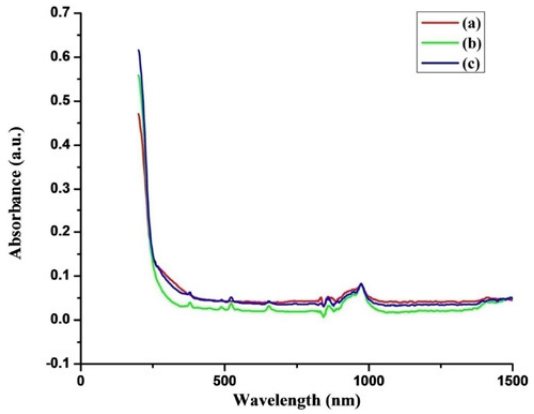

Fig. 6 Absorption spectra obtained for (a) 20%Yb^{3+}/2%Er^{3+}:$NaLuF_4$ and 20%Yb^{3+}/2%Er^{3+} doped $NaLuF_4$ nanocrystals with different Gd^{3+} contents: (b) 20% (c) 45%

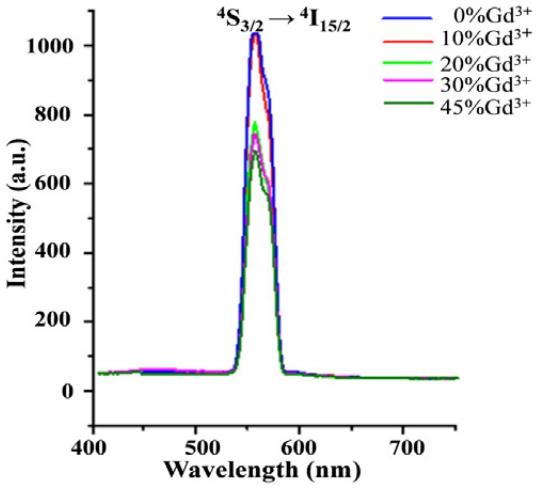

Fig. 7 Emission spectra for 20%Yb^{3+}/2%Er^{3+} doped $NaLuF_4$ nanocrystals with different Gd^{3+} contents monitored at λ_{ex} = 378 nm

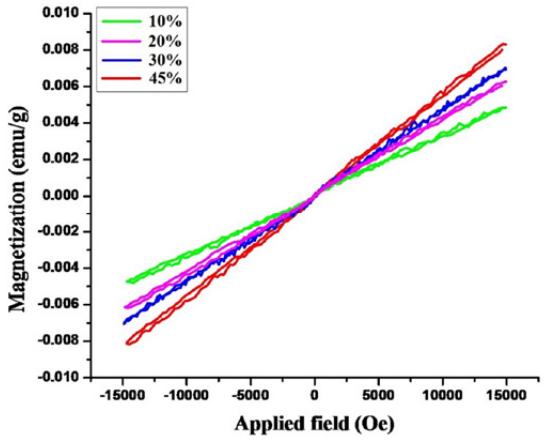

Fig. 8 Magnetization as a function of an applied field for $NaLuF_4$ nanocrystals doped with different Gd^{3+} contents

Down-conversion photoluminescence

The down-conversion emission spectra of $NaLuF_4$:20%Yb^{3+}/2%Er^{3+}/xGd^{3+} (x = 0%, 10%, 20%, 30% and 45%) nanocrystals are shown in Fig. 7. Ytterbium acts as a sensitizer to enhance the luminescent property of erbium dopant ion [54]. Upon excitation at 378 nm, the obtained emission spectrum originates due to transition from the $^4S_{3/2}$ excited state to the $^4I_{15/2}$ ground state of the Er^{3+} ions. With the increase in Gd^{3+} content, the down-conversion (DC) emission intensity of $NaLuF_4$:20%Yb^{3+}/2%Er^{3+}/xGd^{3+} decreases evidently, which is mainly attributed to a significant reduction in the size of $NaLuF_4$ nanocrystals as evident from PXRD and DLS analyses. Decrease in the size of nanocrystals leads to the larger surface quenching sites, hence smaller nanocrystals may suppress DC luminescence by enhanced nonradiative energy transfer processes of the luminescent lanthanide ions [55, 56].

Magnetic properties

Besides the efficient optical property, Gd^{3+} doped $NaLuF_4$ nanocrystals exhibit magnetic properties due to the large magnetic moment of Gd^{3+} at room temperature. Measurement of the magnetization as a function of the applied field (-15 kOe to 15 kOe) for $NaLuF_4$ nanocrystals doped with different Gd^{3+} contents, demonstrate that all the samples present typical paramagnetic behaviour (Fig. 8). The paramagnetic behaviour is mainly attributed to the seven unpaired inner 4f electrons, which are closely bound to the nucleus and effectively shielded by the outer closed shell electrons ($5s^25p^6$) from the crystal field [57]. The magnetization value of the as-prepared $NaLuF_4$ nanocrystals doped with 10%, 20%, 30%, and 45% Gd^{3+} ions are found to be 4.83×10^{-3}, 6.2×10^{-3}, 7.04×10^{-3} and 8.24×10^{-3} emu g^{-1} at 15 kOe, respectively. The magnetization of the $NaLuF_4$ nanocrystals can therefore be modified from 4.83×10^{-3} emu g^{-1} to 8.24×10^{-3} emu g^{-1} at 15 kOe with increasing the Gd^{3+} doping content from 10% to 45%. These results indicate that these multifunctional $NaLuF_4$ nanocrystals may have promising potential applications in bio-separation [58] and magnetic resonance imaging [59].

CONCLUSIONS

In summary, monodispersed Ln^{3+} (Ln = Gd, Yb and Er) doped $NaLuF_4$ nanocrystals were synthesized via a simple hydrothermal method. PXRD analysis reveals that the size of $NaLuF_4$

nanocrystals can be tailored by doping with Gd^{3+}. Increase in the concentration of Gd^{3+} dopant ion can reduce the size of nanocrystal. Besides the efficient optical properties, Gd^{3+} doped $NaLuF_4$ nanocrystals exhibit paramagnetic behaviour at room temperature with magnetization of up to 8.24×10^{-3} emu g^{-1} at 15 kOe, which provides a simple approach for combining two functions into a single phase material. Therefore, the Gd^{3+} doped $NaLuF_4$ nanocrystals not only can control the size but also can integrate additional magnetic functionality into these optical nanomaterials. It is expected that these monodispersed bi-functional $NaLuF_4$ nanocrystals may have potential applications in in vitro and in vivo dual-modal fluorescent, magnetic bio-imaging and bio-separation.

ACKNOWLEDGEMENTS

We are thankful to Human Resource Department (HRD) Group of Council of Scientific & Industrial Research (CSIR) for funding the research fellowship. We would also like to acknowledge Indian Institute of Technology Mandi and Indian Institute of Technology Guwahati for their technical support. We thank SAIF, Panjab University, Chandigarh for powder X-ray diffraction study and we are thankful to Dr. Vinay Kumar, Assistant Professor, School of Physics, Shri Mata Vaishno Devi University (SMVDU) for photoluminescence studies.

CONFLICT OF INTEREST

The authors declare that there is no conflict of interests regarding the publication of this manuscript.

REFERENCES

1. Xu W, Wang Y, Bai X, Dong B, Liu Q, Chen J, et al. Controllable Synthesis and Size-Dependent Luminescent Properties of YVO4:Eu3+ Nanospheres and Microspheres. The Journal of Physical Chemistry C. 2010;114(33):14018-24.
2. Li C, Lin J. Rare earth fluoride nano-/microcrystals: synthesis, surface modification and application. Journal of Materials Chemistry. 2010;20(33):6831-47.
3. Mai H-X, Zhang Y-W, Si R, Yan Z-G, Sun L-d, You L-P, et al. High-Quality Sodium Rare-Earth Fluoride Nanocrystals: Controlled Synthesis and Optical Properties. Journal of the American Chemical Society. 2006;128(19):6426-36.
4. Yu M, Wang H, Lin CK, Li GZ, Lin J. Sol–gel synthesis and photoluminescence properties of spherical SiO 2 @LaPO 4 :Ce 3+ /Tb 3+ particles with a core–shell structure. Nanotechnology. 2006;17(13):3245.
5. Xiaoming Z, Zewei Q, Jun Y, Piaoping Y, Hongzhou L, Jun L. Solvothermal synthesis of well-dispersed MF 2 (M = Ca,Sr,Ba) nanocrystals and their optical properties. Nanotechnology. 2008;19(7):075603.
6. Zhang C, Li C, Peng C, Chai R, Huang S, Yang D, et al. Facile and Controllable Synthesis of Monodisperse CaF2 and CaF2:Ce3+/Tb3+ Hollow Spheres as Efficient Luminescent Materials and Smart Drug Carriers. Chemistry – A European Journal. 2010;16(19):5672-80.
7. Zhang C, Hou Z, Chai R, Cheng Z, Xu Z, Li C, et al. Mesoporous SrF2 and SrF2:Ln3+ (Ln = Ce, Tb, Yb, Er) Hierarchical Microspheres: Hydrothermal Synthesis, Growing Mechanism, and Luminescent Properties. The Journal of Physical Chemistry C. 2010;114(15):6928-36.
8. Gao J, Zhang B, Gao Y, Pan Y, Zhang X, Xu B. Fluorescent Magnetic Nanocrystals by Sequential Addition of Reagents in a One-Pot Reaction: A Simple Preparation for Multifunctional Nanostructures. Journal of the American Chemical Society. 2007;129(39):11928-35.
9. SAFARI J, ZARNEGAR Z. Sulphamic acid-functionalized magnetic Fe3O4 nanoparticles as recyclable catalyst for synthesis of imidazoles under microwave irradiation. Journal of Chemical Sciences. 2013;125(4):835-41.
10. Yu S-Y, Zhang H-J, Yu J-B, Wang C, Sun L-N, Shi W-D. Bifunctional Magnetic–Optical Nanocomposites: Grafting Lanthanide Complex onto Core–Shell Magnetic Silica Nanoarchitecture. Langmuir. 2007;23(14):7836-40.
11. Yu X, Wan J, Shan Y, Chen K, Han X. A Facile Approach to Fabrication of Bifunctional Magnetic-Optical Fe3O4@ZnS Microspheres. Chemistry of Materials. 2009;21(20):4892-8.
12. Shabanian M, Khoobi M, Hemati F, Khonakdar HA, ebrahimi SeS, Wagenknecht U, et al. New PLA/PEI-functionalized Fe3O4 nanocomposite: Preparation and characterization. Journal of Industrial and Engineering Chemistry. 2015;24(Supplement C):211-8.
13. Khoobi M, Khalilvand-Sedagheh M, Ramazani A, Asadgol Z, Forootanfar H, Faramarzi MA. Synthesis of polyethyleneimine (PEI) and β-cyclodextrin grafted PEI nanocomposites with magnetic cores for lipase immobilization and esterification. Journal of Chemical Technology & Biotechnology. 2016;91(2):375-84.
14. Motevalizadeh SF, Khoobi M, Sadighi A, Khalilvand-Sedagheh M, Pazhouhandeh M, Ramazani A, et al. Lipase immobilization onto polyethylenimine coated magnetic nanoparticles assisted by divalent metal chelated ions. Journal of Molecular Catalysis B: Enzymatic. 2015;120:75-83.
15. Khoobi M, Delshad TM, Vosooghi M, Alipour M, Hamadi H, Alipour E, et al. Polyethyleneimine-modified superparamagnetic Fe3O4 nanoparticles: An efficient, reusable and water tolerance nanocatalyst. Journal of Magnetism and Magnetic Materials. 2015;375:217-26.
16. Khoobi M, Motevalizadeh SF, Asadgol Z, Forootanfar H, Shafiee A, Faramarzi MA. Polyethyleneimine-modified superparamagnetic Fe3O4 nanoparticles for lipase immobilization: Characterization and application. Materials Chemistry and Physics. 2015;149–150:77-86.
17. Dalvand A, Nabizadeh R, Reza Ganjali M, Khoobi M, Nazmara S, Hossein Mahvi A. Modeling of Reactive Blue 19 azo dye removal from colored textile wastewater using L-arginine-functionalized Fe3O4 nanoparticles: Optimization, reusability, kinetic and equilibrium studies. Journal of Magnetism and Magnetic Materials. 2016;404(Supplement C):179-89.
18. Fardood ST, Atrak K, Ramazani A. Green synthesis using tragacanth gum and characterization of Ni–Cu–Zn ferrite nanoparticles as a magnetically separable photocatalyst for organic dyes degradation from aqueous solution under visible light. Journal of Materials Science: Materials in Electronics. 2017;28(14):10739-46.
19. Dayyani N, Khoee S, Ramazani A. Design and synthesis of

pH-sensitive polyamino-ester magneto-dendrimers: Surface functional groups effect on viability of human prostate carcinoma cell lines DU145. European Journal of Medicinal Chemistry. 2015;98(Supplement C):190-202.
20. Tarasi R, Khoobi M, Niknejad H, Ramazani A, Ma'mani L, Bahadorikhalili S, et al. β-cyclodextrin functionalized poly (5-amidoisophthalicacid) grafted Fe3O4 magnetic nanoparticles: A novel biocompatible nanocomposite for targeted docetaxel delivery. Journal of Magnetism and Magnetic Materials. 2016;417:451-9.
21. Akrami M, Khoobi M, Khalilvand-Sedagheh M, Haririan I, Bahador A, Faramarzi MA, et al. Evaluation of multilayer coated magnetic nanoparticles as biocompatible curcumin delivery platforms for breast cancer treatment. RSC Advances. 2015;5(107):88096-107.
22. Sadri F, Ramazani A, Massoudi A, Khoobi M, Azizkhani V, Tarasi R, et al. Magnetic CoFe2O4 nanoparticles as an efficient catalyst for the oxidation of alcohols to carbonyl compounds in the presence of oxone as an oxidant. Bull Korean Chem Soc. 2014;35(7):2029.
23. Sadri F, Ramazani A, Massoudi A, Khoobi M, Tarasi R, Shafiee A, et al. Green oxidation of alcohols by using hydrogen peroxide in water in the presence of magnetic Fe3O4 nanoparticles as recoverable catalyst. Green Chemistry Letters and Reviews. 2014;7(3):257-64.
24. Ramazani A, Sadri F, MASSOUDI A, Khoobi M, Joo SW, Dolatyari L, et al. Magnetic ZnFe2O4 nanoparticles as an efficient catalyst for the oxidation of alcohols to carbonyl compounds in the presence of oxone as an oxidant. Iranian Journal of Catalysis. 2015;5(3):285-91.
25. Sadri F, Ramazani A, Massoudi A, Khoobi M, Joo S. Magnetic CuFe2O4 nanoparticles as an efficient catalyst for the oxidation of alcohols to carbonyl compounds in the presence of oxone as an oxidant. Bulgarian Chemical Communications. 2015;47(2):539-46.
26. Sadri F, Ramazani A, Ahankar H, Taghavi Fardood S, Azimzadeh Asiabi P, Khoobi M, et al. Aqueous-phase oxidation of alcohols with green oxidants (Oxone and hydrogen peroxide) in the presence of MgFe2O4 magnetic nanoparticles as an efficient and reusable catalyst. Journal of Nanostructures. 2016;6(4):264-72.
27. Tarasi R, Ramazani A, Ghorbanloo M, Khoobi M, Aghahosseini H, Joo SW, et al. Preparation and Characterization of MCM-41@PEI-Mn as a New Organic–Inorganic Hybrid Nanomaterial and Study of its Catalytic Role in the Oxidation of Cyclohexene, Ethyl Benzene, and Toluene in the Presence of H2O2 as an Oxidant. Bulletin of the Korean Chemical Society. 2016;37(4):529-37.
28. Khoobi M, Ramazani A, Hojjati Z, Shakeri R, Khoshneviszadeh M, Ardestani SK, et al. Synthesis of Novel 4H-Chromenes Containing a Pyrimidine-2-Thione Function in the Presence of Fe3O4 Magnetic Nanoparticles and Study of Their Antioxidant Activity. Phosphorus, Sulfur, and Silicon and the Related Elements. 2014;189(10):1586-95.
29. Fardood ST, Ramazani A, Moradi S. Green synthesis of Ni–Cu–Mg ferrite nanoparticles using tragacanth gum and their use as an efficient catalyst for the synthesis of polyhydroquinoline derivatives. Journal of Sol-Gel Science and Technology. 2017;82(2):432-9.
30. Taghavi Fardood S, Ramazani A, Golfar Z, Joo SW. Green synthesis of Ni-Cu-Zn ferrite nanoparticles using tragacanth gum and their use as an efficient catalyst for the synthesis of polyhydroquinoline derivatives. Applied Organometallic Chemistry. 2017:e3823-n/a.
31. Chan Y, Zimmer JP, Stroh M, Steckel JS, Jain RK, Bawendi MG. Incorporation of Luminescent Nanocrystals into Monodisperse Core–Shell Silica Microspheres. Advanced Materials. 2004;16(23-24):2092-7.
32. Deng YH, Yang WL, Wang CC, Fu SK. A Novel Approach for Preparation of Thermoresponsive Polymer Magnetic Microspheres with Core–Shell Structure. Advanced Materials. 2003;15(20):1729-32.
33. Salgueiriño-Maceira V, Correa-Duarte MA, Spasova M, Liz-Marzán LM, Farle M. Composite Silica Spheres with Magnetic and Luminescent Functionalities. Advanced Functional Materials. 2006;16(4):509-14.
34. Meng X, Li H, Chen J, Mei L, Wang K, Li X. Mössbauer study of cobalt ferrite nanocrystals substituted with rare-earth Y3+ ions. Journal of Magnetism and Magnetic Materials. 2009;321(9):1155-8.
35. Zi Z, Sun Y, Zhu X, Yang Z, Dai J, Song W. Synthesis and magnetic properties of CoFe2O4 ferrite nanoparticles. Journal of Magnetism and Magnetic Materials. 2009;321(9):1251-5.
36. Phua LX, Xu F, Ma YG, Ong CK. Structure and magnetic characterizations of cobalt ferrite films prepared by spray pyrolysis. Thin Solid Films. 2009;517(20):5858-61.
37. Kashevsky BE, Agabekov VE, Kashevsky SB, Kekalo KA, Manina EY, Prokhorov IV, et al. Study of cobalt ferrite nanosuspensions for low-frequency ferromagnetic hyperthermia. Particuology. 2008;6(5):322-33.
38. Laroche M, Girard S, Moncorgé R, Bettinelli M, Abdulsabirov R, Semashko V. Beneficial effect of Lu3+ and Yb3+ ions in UV laser materials. Optical Materials. 2003;22(2):147-54.
39. Cheng X, Zhang S, Xu J, Peng H, Hang Y. High-power diode-end-pumped Tm:LiLuF4 slab lasers. Optics Express. 2009;17(17):14895-901.
40. Jia G, Zheng Y, Liu K, Song Y, You H, Zhang H. Facile Surfactant- and Template-Free Synthesis and Luminescent Properties of One-Dimensional Lu2O3:Eu3+ Phosphors. The Journal of Physical Chemistry C. 2009;113(1):153-8.
41. Shi F, Wang J, Zhai X, Zhao D, Qin W. Facile synthesis of [small beta]-NaLuF4 : Yb/Tm hexagonal nanoplates with intense ultraviolet upconversion luminescence. CrystEngComm. 2011;13(11):3782-7.
42. Li C, Quan Z, Yang J, Yang P, Lin J. Highly Uniform and Monodisperse β-NaYF4:Ln3+ (Ln = Eu, Tb, Yb/Er, and Yb/Tm) Hexagonal Microprism Crystals: Hydrothermal Synthesis and Luminescent Properties. Inorganic Chemistry. 2007;46(16):6329-37.
43. Li C, Yang J, Quan Z, Yang P, Kong D, Lin J. Different Microstructures of β-NaYF4 Fabricated by Hydrothermal Process: Effects of pH Values and Fluoride Sources. Chemistry of Materials. 2007;19(20):4933-42.
44. Wang X, Peng Q, Li Y. Interface-Mediated Growth of Monodispersed Nanostructures. Accounts of Chemical Research. 2007;40(8):635-43.
45. Chen G, Ohulchanskyy TY, Kachynski A, Ågren H, Prasad PN. Intense Visible and Near-Infrared Upconversion Photoluminescence in Colloidal LiYF4:Er3+ Nanocrystals under Excitation at 1490 nm. ACS Nano. 2011;5(6):4981-6.
46. Teng X, Zhu Y, Wei W, Wang S, Huang J, Naccache R, et al. Lanthanide-Doped NaxScF3+x Nanocrystals: Crystal Structure Evolution and Multicolor Tuning. Journal of the American Chemical Society. 2012;134(20):8340-3.
47. Shang M, Li G, Kang X, Yang D, Geng D, Peng C, et al. LaOF : Eu3+ nanocrystals: hydrothermal synthesis, white and color-tuning emission properties. Dalton Transactions. 2012;41(18):5571-80.
48. Shang M, Geng D, Kang X, Yang D, Zhang Y, Lin J.

Hydrothermal Derived LaOF:Ln3+ (Ln = Eu, Tb, Sm, Dy, Tm, and/or Ho) Nanocrystals with Multicolor-Tunable Emission Properties. Inorganic Chemistry. 2012;51(20):11106-16.
49. He M, Huang P, Zhang C, Hu H, Bao C, Gao G, et al. Dual Phase-Controlled Synthesis of Uniform Lanthanide-Doped NaGdF4 Upconversion Nanocrystals Via an OA/Ionic Liquid Two-Phase System for In Vivo Dual-Modality Imaging. Advanced Functional Materials. 2011;21(23):4470-7.
50. Zhou J, Zhu X, Chen M, Sun Y, Li F. Water-stable NaLuF4-based upconversion nanophosphors with long-term validity for multimodal lymphatic imaging. Biomaterials. 2012;33(26):6201-10.
51. Li F, Li C, Liu X, Chen Y, Bai T, Wang L, et al. Hydrophilic, Upconverting, Multicolor, Lanthanide-Doped NaGdF4 Nanocrystals as Potential Multifunctional Bioprobes. Chemistry – A European Journal. 2012;18(37):11641-6.
52. Niu N, He F, Huang S, Gai S, Zhang X, Yang P. Hierarchical bundles structure of [small beta]-NaLuF4: facile synthesis, shape evolution, and luminescent properties. RSC Advances. 2012;2(27):10337-44.
53. He F, Niu N, Wang L, Xu J, Wang Y, Yang G, et al. Influence of surfactants on the morphology, upconversion emission, and magnetic properties of [small beta]-NaGdF4:Yb3+,Ln3+ (Ln = Er, Tm, Ho). Dalton Transactions. 2013;42(27):10019-28.
54. Wang F, Han Y, Lim CS, Lu Y, Wang J, Xu J, et al. Simultaneous phase and size control of upconversion nanocrystals through lanthanide doping. Nature. 2010;463(7284):1061-5.
55. Wang F, Wang J, Liu X. Direct Evidence of a Surface Quenching Effect on Size-Dependent Luminescence of Upconversion Nanoparticles. Angewandte Chemie International Edition. 2010;49(41):7456-60.
56. Wong H-T, Chan HL, Hao J. Magnetic and luminescent properties of multifunctional GdF 3: Eu 3+ nanoparticles. Applied physics letters. 2009;95(2):022512.
57. Liu Z, Yi G, Zhang H, Ding J, Zhang Y, Xue J. Monodisperse silica nanoparticles encapsulating upconversion fluorescent and superparamagnetic nanocrystals. Chemical Communications. 2008(6):694-6.
58. Estelrich J, Sánchez-Martín MJ, Busquets MA. Nanoparticles in magnetic resonance imaging: from simple to dual contrast agents. International Journal of Nanomedicine. 2015;10:1727-41.
59. Yu T, Joo J, Park YI, Hyeon T. Large-Scale Nonhydrolytic Sol–Gel Synthesis of Uniform-Sized Ceria Nanocrystals with Spherical, Wire, and Tadpole Shapes. Angewandte Chemie International Edition. 2005;44(45):7411-4.